Appl. Phys. B (2008)
DOI: 10.1007/s00340-008-2989-3

Applied Physics B
Lasers and Optics

K. BRANDS[1]
M. FALK[1]
D. HAERTLE[1]
T. WOIKE[2]
K. BUSE[1,✉]

Impedance spectroscopy of iron-doped lithium niobate crystals

[1] Institute of Physics, University of Bonn, 53115 Bonn, Germany
[2] Institute for Mineralogy, University of Cologne, 50674 Köln, Germany

Received: 18 February 2008

ABSTRACT The dc conductivity of as-grown and oxidized iron-doped lithium niobate crystals is measured by impedance spectroscopy in the temperature range 30–700 °C. Electron and ion conduction at lower and higher temperatures are clearly distinguished, providing relevant information for understanding and optimizing the recently developed thermo-electric oxidization that makes crystals robust against optical damage.

PACS 77.84.Dy; 72.20.Fr

1 Introduction

Lithium niobate ($LiNbO_3$) crystals are promising for various applications, e.g. nonlinear-optical frequency conversion and holographic frequency filtering [1, 2]. While for holographic applications the photorefractive effect is a prerequisite and is deliberately enhanced by adding dopants [3], for nonlinear-optical applications photorefraction is undesired, since it disturbs the beam shape and the phase-matching conditions at high light intensities. This so-called 'optical damage' occurs also in nominally undoped lithium niobate, where mainly remaining iron impurities in valence states 2+ and 3+ act as electron sources and electron traps, respectively. Excitation of electrons from Fe^{2+} with light causes a subsequent migration of these charge carriers into other areas where they are trapped by Fe^{3+} centers. The resulting space-charge field induces a refractive-index change via the electro-optic effect.

A method published recently [4], thermo-electric oxidization, allows nearly complete oxidization of the Fe^{2+} impurities to Fe^{3+}. This oxidization process diminishes the optical damage of undoped congruent lithium niobate crystals by at least one order of magnitude [5], and allowed periodically poled crystals to generate 100 times more power by second-harmonic generation [6]. Iron-doped crystals can be oxidized by this method as well, which allows us to study the underlying process [7].

✉ Fax: +49-228-73-40-38, E-mail: kbuse@uni-bonn.de
The online version of this article (doi:10.1007/s00340-008-2989-3) contains supplementary material, which is available to authorized users.

In this article we analyze the changes of the dc conductivity caused by the thermo-electric oxidization process. Knowledge about the conductivities at the temperature of the thermo-electric oxidization is essential for modeling and optimization of this process.

The Fe^{2+} concentration remaining after the thermo-electric oxidization is too small to be determined by absorption spectroscopy [7]. The dependence of the bulk photovoltaic current on $c_{Fe^{2+}}$ has been used to determine these extreme degrees of oxidization in thermo-electrically oxidized $LiNbO_3$ crystals [7]. However, an independent and non-optical proof of these results is still needed. In this contribution we describe a simple way to determine the degree of the oxidization for the highly-iron-doped crystals after such an oxidization process.

2 Experimental methods

We examine congruent lithium niobate crystals from Crystal Technology, Inc. with several iron-doping levels (nominally undoped and with 0.05, 0.5, 1, and 2 wt. % Fe_2O_3 added to the melt). The incorporation of iron is tested by atomic absorption spectroscopy for the three most heavily doped samples, and is 0.368, 0.670, and 1.11 wt. % Fe_2O_3 in the crystal, respectively. For some experiments a nearly stoichiometric crystal from Oxide Corp. is also used, which is doped with 0.03 wt. % Fe_2O_3. The crystals are cut into x plates of the dimensions 0.1–0.6 mm × 11 mm × 11 mm. For each iron concentration a crystal undergoes the thermo-electric oxidization treatment [4], and a reference sample is kept in the as-grown state. In addition, one crystal (0.5 wt. % Fe_2O_3) is oxidized in the conventional way, by annealing for 12 h in a dry oxygen atmosphere at 1000 °C. For the samples with this iron concentration the hydrogen concentration is determined by measuring the absorption of the OH^- line at 2.87 μm [8]. A 100-nm-thick gold electrode is evaporated on both x sides of the crystal, with an intermediate layer of 10-nm chromium for better adhesion to the crystal. The size of the electrode and of the intermediate layer is 10 mm × 10 mm.

Impedance spectra in the frequency range from $\omega/2\pi = 10^{-2}$ Hz to 3×10^5 Hz are taken with a spectrometer (Alpha L from Novocontrol). The temperature is stabilized to ±0.5 °C by a self-built oven allowing measurements in the temperature range 30–700 °C.

3 Results and discussion

From the spectra of the complex impedance we derive the real part $\sigma(\omega)$ of the complex conductivity [9] over the measured frequency range. Typical conductivity spectra are shown in Fig. 1. The high density of intrinsic defects and iron impurities in lithium niobate crystals allows us to use the 'random free energy barrier model' [10] to describe the conductivity. This model assumes that the charge carriers perform a random walk in a randomly disordered potential landscape. The conductivity is predicted to saturate to the dc level σ_{dc} for small frequencies, with the dependence

$$\sigma(\omega) = \sigma_{\mathrm{dc}} \frac{\omega\tau_{\mathrm{e}} \arctan(\omega\tau_{\mathrm{e}})}{\frac{1}{4}\ln^2\left(1+\omega^2\tau_{\mathrm{e}}^2\right) + \arctan^2(\omega\tau_{\mathrm{e}})}, \quad (1)$$

where $1/\tau_{\mathrm{e}}$ is a frequency indicating when the conductivity has nearly reached the dc level ($\sigma(1/\tau_{\mathrm{e}}) \approx 1.066\sigma_{\mathrm{dc}}$). We fit (1) to the measured conductivity spectra and obtain the parameters σ_{dc} and τ_{e}. Figure 2 shows σ_{dc} plotted versus the inverse temperature for crystals that have undergone different oxidizing treatments. In this plot the branches with constant activation energy in the Arrhenius expression

$$\sigma_{\mathrm{dc}}(T) = \sigma_0 \exp\left(-\frac{E_{\mathrm{A}}}{k_{\mathrm{B}}T}\right) \quad (2)$$

appear as straight lines. Two different activation energies can be seen: for lower temperatures σ_{dc} depends on the oxidization state, i.e. on the Fe^{2+} concentration $c_{\mathrm{Fe}^{2+}}$. Charge transport in the low-temperature branch, with an activation energy $E_{\mathrm{A}} \approx 0.35$ eV, can therefore be attributed to electrons. In the high-temperature range (350–700 °C), the crystals in different oxidization states show a similar dc conductivity, with an activation energy $E_{\mathrm{A}} \approx 1.2$ eV. This branch comes from ionic conduction. We can rule out thermally excited electrons, since the conductivity in this branch does not depend strongly on the iron concentration, i.e. on the availability of electrons (see Fig. 3), and the band gap is too large for thermal excitation of electron–hole pairs. The conducting ions can be either hydrogen or lithium ions. Both have a similar activation energy with literature values varying from 0.95 to 1.33 eV for hydrogen [11–14] and from 1.17 to 1.25 eV for lithium ions [15, 16], and both can have a similar contribution to the dc conductivity in this temperature range for typical hydrogen concentrations [17]. Although not enough to discriminate, our data points to Li^+ as the moving ions: on the one hand we measured a 20% smaller activation energy in stoichiometric $LiNbO_3$, which has a different Li concentration, and on the other hand we do not see a strong dependence of the conductivity on the hydrogen concentration, which varies by a factor of 50 in the crystals used in Fig. 2.

Figure 4 shows a summary of the activation energies obtained from (2) for as-grown and thermo-electrically oxidized crystals versus the iron concentration, for the high- and low-temperature branches. The ionic activation energy, i.e. the activation energy of the high-temperature branches, depends on the oxidization state, and for as-grown crystals it depends also on the iron concentration. Klauer et al. measuring the activation energy for two iron concentrations (undoped and 0.032 wt. %) found the same trend [13]. For the thermo-electrically oxidized samples we measure a constant activation energy of $E_{\mathrm{A}} = (1.13 \pm 0.09)$ eV over the iron-doping range of Fig. 4.

For lower temperatures and with nominal iron concentration $c_{\mathrm{Fe}} \geq 0.5$ wt. %, the conductivity is dominated by elec-

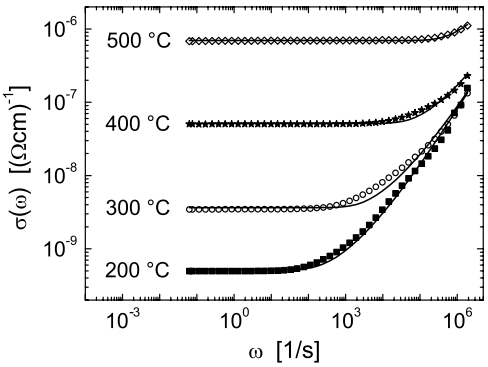

FIGURE 1 Conductivity spectra of an as-grown $LiNbO_3$ crystal doped with 0.5 wt. % Fe_2O_3 in the melt. For low frequencies the conductivity saturates to the value of the dc conductivity σ_{dc}. The *lines* are fits according to (1)

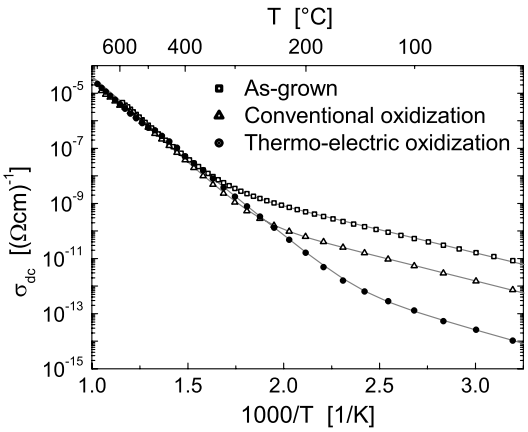

FIGURE 2 Arrhenius plot of the dc conductivity of an as-grown, a conventionally oxidized, and a thermo-electrically oxidized crystal. The crystals are doped with 0.5 wt. % Fe_2O_3. The *continuous lines* are fits with two contributions of the form of (2). The fit parameters are given in the electronic supplementary material

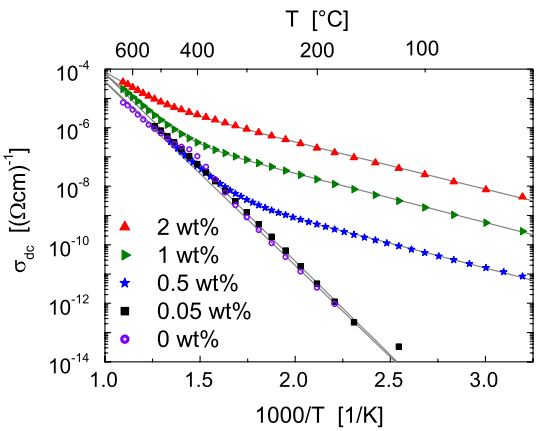

FIGURE 3 Arrhenius plot of the dc conductivity of as-grown $LiNbO_3$ samples with various iron-doping concentrations, in wt. % Fe_2O_3 in the melt. Fit parameters for the *continuous lines* are given in the electronic supplementary material

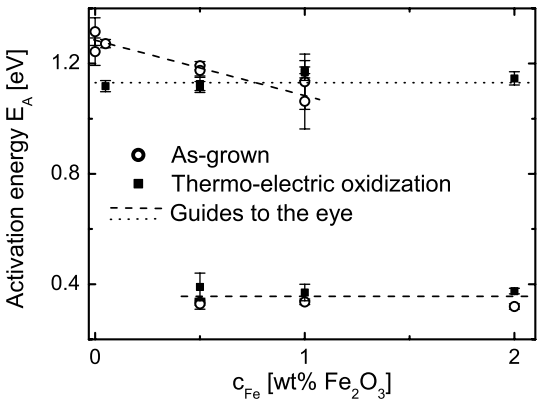

FIGURE 4 Activation energies of as-grown (*empty circles*) and thermo-electrically oxidized (*black squares*) lithium niobate crystals versus the iron concentration, in wt. % Fe_2O_3 in the melt. The activation energies for ionic conduction ($E_A \approx 1.2$ eV) and for electronic conduction ($E_A \approx 0.35$ eV) are connected by *straight lines* as guides to the eye

trons, and the activation energy is independent of the iron concentration. For as-grown samples we have $E_A = (0.33 \pm 0.03)$ eV, while for oxidized samples it is only slightly higher, with $E_A = (0.38 \pm 0.05)$ eV. For lower iron concentrations the ionic conductivity remains dominant until our detection limit of $\sigma = 10^{-14}\ \Omega^{-1}\,\mathrm{cm}^{-1}$ is reached. The indicated error in the activation energy is determined by the spread of the measured values.

4 Oxidation state of the iron impurities

By using the dc conductivity from the electronic branch we calculate the ratio of the Fe^{2+} concentration to the total iron concentration for the thermo-electrically oxidized samples. In lithium niobate with high iron doping ($c_{Fe} \geq 0.05$ wt. %) the dominant charge transport at room temperature is given by tunneling of electrons between iron sites [18, 19]. The conductivity is proportional to the effective number of defects,

$$\sigma_{dc} \propto \frac{c_{Fe^{2+}} c_{Fe^{3+}}}{c_{Fe}} . \qquad (3)$$

Taking the ratio $\sigma_{dc,ox}/\sigma_{dc,as\text{-}gr.}$ eliminates the proportionality constant in (3) and, with $c_{Fe^{2+},ox} \ll c_{Fe^{3+},ox}$ [7], we obtain

$$\frac{c_{Fe^{2+},ox}}{c_{Fe}} = \frac{\sigma_{dc,ox}}{\sigma_{dc,as\text{-}gr.}} \frac{c_{Fe^{2+},as\text{-}gr.}}{c_{Fe}} \frac{c_{Fe^{3+},as\text{-}gr.}}{c_{Fe}} . \qquad (4)$$

For the crystals with nominal iron concentration ≥ 0.5 wt. % we could measure the electronic conductivity for both oxidization states. The ratios of the electronic dc conductivities and the resulting concentration ratios $c_{Fe^{2+}}/c_{Fe}$ for the thermo-electrically oxidized crystals are given in Table 1. The

c_{Fe} [wt. %]	$c_{Fe^{2+}}/c_{Fe}$ as-grown	$\frac{\sigma_{dc,ox}}{\sigma_{dc,as\text{-}gr.}}$	$c_{Fe^{2+}}/c_{Fe}$ oxidized
0.5	0.20 ± 0.05	$(1.5 \pm 0.3) \times 10^{-3}$	$(2.4 \pm 1) \times 10^{-4}$
1.0	0.18 ± 0.05	$(3.3 \pm 0.7) \times 10^{-5}$	$(5 \pm 2) \times 10^{-6}$
2.0	0.18 ± 0.05	$(4.5 \pm 0.9) \times 10^{-5}$	$(7 \pm 3) \times 10^{-6}$

TABLE 1 Concentration ratios $c_{Fe^{2+}}/c_{Fe}$ for as-grown $LiNbO_3$, determined by absorption spectroscopy, and thermo-electrically oxidized $LiNbO_3$, determined by the measured ratio of dc conductivities and (4). The iron concentration c_{Fe} is given in wt. % Fe_2O_3 in the melt

determined values are smaller but not too far off from the concentration ratios determined in [7] by the bulk photovoltaic current, and show the performance of the thermo-electric oxidization, which is orders of magnitude stronger than the one obtainable with conventional oxidization. Regarding absolute oxidization values, one has also to consider that the annealing depends on plenty of parameters and hence the outcomes can vary from run to run easily. For example, the thermo-electrically oxidized sample doped with 0.5 wt. % Fe shows some inhomogeneities that could explain its relatively large $c_{Fe^{3+}}/c_{Fe}$ ratio.

In summary, we showed that dc conductivity data of $LiNbO_3$ crystals allows us to gain insights into the optical damage suppression by the thermo-electric annealing.

ACKNOWLEDGEMENTS The authors thank D.R. Evans and S.A. Basun for discussions.

REFERENCES

1 L. Arizmendi, Phys. Stat. Solidi A **201**, 253 (2004)
2 P. Boffi, D. Piccinin, M.C. Ubaldi (eds.), *Infrared Holography for Optical Communications* (Springer, Berlin, 2003)
3 K. Buse, Appl. Phys. B **64**, 391 (1997)
4 M. Falk, K. Buse, Appl. Phys. B **81**, 853 (2005)
5 M. Falk, T. Woike, K. Buse, Appl. Phys. Lett. **90**, 251 (2007)
6 I. Breunig, M. Falk, B. Knabe, R. Sowade, K. Buse, P. Rabiei, D.H. Jundt, Appl. Phys. Lett. **91**, 221 (2007)
7 M. Falk, J. Japs, T. Woike, K. Buse, Appl. Phys. B **87**, 119 (2007)
8 J.M. Cabrera, J. Olivares, M. Carrascosa, J. Rams, R. Müller, E. Diguez, Adv. Phys. **45**, 349 (1996)
9 F. Kremer, A. Schönhals, *Broadband Dielectric Spectroscopy* (Springer, Berlin, 2003)
10 J.C. Dyre, J. Appl. Phys. **64**, 2456 (1988)
11 E.M. de Miguel-Sanz, M. Carrascosa, L. Arizmendi, Phys. Rev. B **65**, 165 (2002)
12 Y.P. Yang, I. Nee, K. Buse, D. Psaltis, Appl. Phys. Lett. **78**, 4076 (2001)
13 S. Klauer, M. Wohlecke, S. Kapphan, Phys. Rev. B **45**, 2786 (1992)
14 S. Carrascosa, L. Arizmendi, J. Appl. Phys. **73**, 2709 (1993)
15 D.P. Birnie, J. Mater. Sci. **28**, 302 (1993)
16 H. Franke, Phys. Stat. Solidi A **83**, K73 (1984)
17 I. Nee, K. Buse, F. Havermeyer, R.A. Rupp, M. Fally, R.P. May, Phys. Rev. B **60**, R9896 (1999)
18 I. Nee, M. Müller, K. Buse, E. Krätzig, J. Appl. Phys. **88**, 4282 (2000)
19 J.C. Dyre, T.B. Schroder, Rev. Mod. Phys. **72**, 873 (2000)